Control of an electric diwheel

B. Cazzolato, J. Harvey, C. Dyer, K. Fulton, E. Schumann, C. Zhu and Z. Prime
University of Adelaide, Australia
benjamin.cazzolato@adelaide.edu.au

Abstract

A diwheel is a novel vehicle consisting of two large outer wheels which completely encompass an inner frame. The inner frame freely rotates inside the wheels using supporting idler wheels. The outer wheels are driven from the inner frame and forward motion is achieved through a reaction torque generated by the eccentricity of the centre of gravity of the inner frame. During operation, diwheels experience slosh (when the inner frame oscillates) and tumbling (when the inner frame completes a revolution). In this paper the dynamics of a generic diwheel are derived. Three control strategies are then proposed; slosh control, swing-up control and inversion control. Finally, simulations are conducted on a model of a diwheel currently under construction at the University of Adelaide.

1 Introduction

The diwheel is a device which consists of a two large outer wheels which completely encompass an inner frame. The inner frame is free to rotate within the wheels, and is typically supported by a common axle or idlers which roll on the wheels (see Figure 1). Diwheels, like their more popular cousins the monowheel, have been around for almost one and a half centuries [Self, accessed Aug 2009; Cardini, 2006]. All of these platforms suffer from two common issues affecting driver comfort; slosh and tumbling (also known as gerbilling). Sloshing is when the inner frame oscillates, and it occurs in all monowheels and diwheels where the centre of gravity of the inner frame is offset from the centre line of the wheels. It is very prevalent as these platforms typically have low damping between the wheel and the frame in order to minimise power consumption during locomotion. In addition, during severe braking or acceleration the inner frame will tumble relative to the earth centred frame, which obviously affects the ability of the driver to control the platform.

In March 2009, honours students in the School of Mechanical Engineering, at the University of Adelaide commenced the design and build of an electric diwheel. The vehicle was called EDWARD (Electric DiWheel with Active Rotation Damping) [DYER *et al.*, 2009]. A rendered solid model of the platform is shown in Figure 1 and Figure 2 shows the current stage of construction of the platform. The outer wheels are rolled and welded stainless steel tube with a rubber strip bonded on the outer rolling surface. An inner frame supports the driver who is held in place by a five-point racing harness. The inner frame runs on the outer wheels with three nylon idlers and is coupled to the inner frame by suspension arms, which act to provide some suspension and also maintain a constant contact force between the idlers and the wheel. Two brushed DC motors each drive (via sprockets and a chain) a small motor cycle drive-wheel which contacts the inner radius of the outer wheel. Thus the vehicle can be driven forwards and backwards using a collective voltage in to the motors, and can be yawed when the motors are differentially driven. The vehicle is drive-by-wire, and the driver controls the vehicle via a joystick. There is also a mechanical foot brake which operates calipers on the drive-wheels (in case of electrical failure). There are three sensing systems on board, viz. a solid state gyroscope (for measuring pitch rate), a solid state DC coupled accelerometer (for state estimation of pitch angle) and incremental encoders on the two drive-wheels.

The scope of the project was to not only design and build the mechanical and electrical platform, but to also implement several control strategies to modify the dynamics. The first was a slosh controller, with the purpose of minimising the rocking motion that occurs as the vehicle is accelerated or decelerated when torquing the drive motors. This was deemed necessary after viewing videos of monowheels and diwheels in operation. If implemented correctly it would also allow maximum deceleration of the vehicle if necessary, which occurs when the centre of gravity of the inner frame is horizontally aligned

Figure 1: Rendered image of the EDWARD diwheel

Figure 2: Photograph of the EDWARD diwheel during construction

to the centre of the outer wheels. Another control mode was also considered with the aim to make the ride in the vehicle more exciting. This involved a swing-up controller followed by an inversion controller. The purpose of this controller was to invert the driver, then stabilise them enabling them to drive around upside down.

In this paper the dynamics of a generic diwheel using a Lagrangian formulation are derived. The control laws for the two control strategies are presented. Details of the EDWARD diwheel and its parameters are used in a numerical simulation, for which the open loop response and various closed loop responses are presented. Finally suggestions for future control strategies are made.

2 Dynamics of the 2DOF system

In the derivation of the diwheel dynamics that follows, motion has been restricted to the xy-plane. In this two degree-of-freedom model, the left and right wheel and left and right drive-wheels are combined into a single degree of freedom. In this way both pairs of wheels and drive-wheels rotate at equal speeds so that the diwheel does not yaw about the y-axis. A Lagrangian approach has been used for the derivation of the dynamic model of the diwheel, similar to that of shown in [Martynenko and Formal'skii, 2005].

The following assumptions have been made in the derivation of the dynamics.

- The motion is restricted to the xy-plane.
- Friction is limited to viscous friction, and the Coulomb friction arising from the idler rollers is neglected.
- The suspension arms are fixed, keeping the centre of gravity of the inner frame a fixed distance from the centre of the wheels.
- The inductance of the motor is negligible and therefore the current is an algebraic function of voltage and motor speed.
- The rotational and translational inertia from the motors and drive-wheels has been included in the inner frame.
- There is no slip between the drive-wheels and the outer wheels.
- There is no slip between the outer wheels and the ground.

The model has three coordinates, however the latter two are dependent:

- θ - rotation of the inner frame assembly about the z-axis.
- $\varphi_L = \varphi_R = \varphi$ - rotation of the wheels about the z-axis.
- x - the displacement of the diwheel (centre) about an earth centred frame.

The right-handed coordinate frame is located at the centre of rotation of the diwheel, as shown in Figure 3. The positive x-direction is to the right and positive y is down. Clockwise rotations about the centre are considered positive. The zero datum for the measurement of both the body angle θ and wheel angle φ is coincident with the positive y-axis.

Since the drive-wheel is fixed to the inner frame (body 2) the two masses may be lumped together. However, in the development that follows, the energy associated with the rotational velocity of the drive-wheel is omitted, as it is considered negligible.

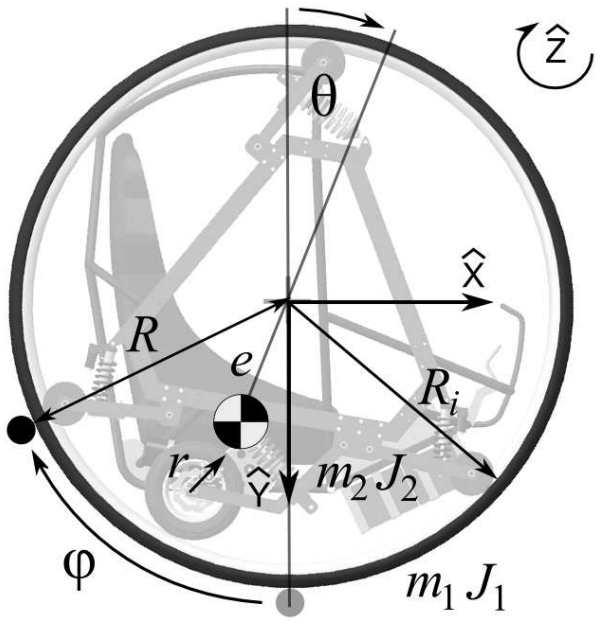

Figure 3: Schematic of a generic diwheel showing coordinate systems, mass distributions and states.

2.1 Non-linear dynamics

The Euler-Lagrange equations yield the dynamic model in terms of energy and are given by

$$\frac{d}{dt}\left(\frac{\partial L}{\partial \dot{q}_i}\right) - \frac{\partial L}{\partial q_i} = F_i \tag{1}$$

where the Lagrangian L is an expression of the difference in the kinetic and potential energies of the system, q_i are generalised coordinates (in this case θ and φ) and F_i are generalised forces. The solution of the Lagrange equation for each coordinate, q_i, yields an expression of the form:

$$\mathbf{M(q)\ddot{q} + C(q,\dot{q}) + G(q) = F} \tag{2}$$

which summarise the system dynamics.

Velocities

The translational and rotational velocities of the bodies comprising the diwheel are presented below in preparation for the Lagrangian. The translational velocity of the wheel (body 1) in the x-direction is

$$v_{1x} = R\,\dot{\varphi}, \tag{3}$$

where R is the outer wheel radius and $\dot{\varphi}$ is the angular velocity of the wheel. The translational velocity in x-direction of the CoG of body 2 (the inner frame) is

$$v_{2x} = R\,\dot{\varphi} - \dot{\theta}\,e\,\cos(\theta)\,, \tag{4}$$

where e is the eccentricity between the inner frame CoG and the centre of the wheels, and $\dot{\theta}$ is the angular velocity of the inner frame relative to an earth centred frame. The corresponding velocity in y-direction of the inner frame CoG is

$$v_{2y} = -\dot{\theta}\,e\,\sin(\theta)\,. \tag{5}$$

The magnitude of the velocity of the inner frame CoG is thus

$$|v_2| = \left(\left(R\,\dot{\varphi} - \dot{\theta}\,e\,\cos(\theta)\right)^2 + \dot{\theta}^2\,e^2\,\sin(\theta)^2\right)^{\frac{1}{2}}. \tag{6}$$

Kinetic Energy

The kinetic energy of the diwheel has been separated into the following terms. First, the rotational energy of the wheel,

$$E_{1r} = \frac{J_1\,\dot{\varphi}^2}{2}, \tag{7}$$

where J_1 is the *combined* moment of inertia of both wheels about their centre.

Second, the translational energy of the wheel,

$$E_{1t} = \frac{R^2\,\dot{\varphi}^2\,m_1}{2}, \tag{8}$$

where m_1 is the *combined* mass of both wheels.

Third, the rotational energy of the inner frame,

$$E_{2r} = \frac{J_2\,\dot{\theta}^2}{2}, \tag{9}$$

where J_2 is the moment of inertia of the inner frame about its CoG.

Lastly, the translational energy of the inner frame CoG,

$$\begin{aligned} E_{2t} &= \frac{1}{2}m_2 v_2^2 \\ &= \frac{m_2\left(\left(R\,\dot{\varphi} - \dot{\theta}\,e\,\cos(\theta)\right)^2 + \dot{\theta}^2\,e^2\,\sin^2(\theta)\right)}{2}, \end{aligned} \tag{10}$$

where m_2 is the mass of the inner frame and $N = \frac{R}{r}$ is the ratio of outer wheel radius R to drive-wheel radius r.

Thus the total kinetic energy of this system is:

$$\begin{aligned} E_k &= E_{1r} + E_{1t} + E_{2r} + E_{2t} \\ &= \frac{m_2\left(\left(R\,\dot{\varphi} - \dot{\theta}\,e\,\cos(\theta)\right)^2 + \dot{\theta}^2\,e^2\,\sin^2(\theta)\right)}{2} \\ &\quad + \frac{J_1\,\dot{\varphi}^2}{2} + \frac{J_2\,\dot{\theta}^2}{2} + \frac{R^2\,\dot{\varphi}^2\,m_1}{2}. \end{aligned} \tag{11}$$

Potential Energy

The potential energy of the wheel is zero. Therefore the total potential energy (assuming zero potential energy at $\theta = 0$) is related to the change in height of the CoG of the inner frame and is given by

$$E_p = e\, g\, m_2\, (1 - \cos(\theta)), \tag{12}$$

where g is the gravitational acceleration.

Lagrangian

The Lagrangian for the diwheel is the difference in the kinetic and potential energies, $E_k - E_p$,

$$\begin{aligned} L &= \left(\frac{J_1}{2} + \frac{R^2\, m_1}{2} + \frac{R^2\, m_2}{2}\right) \dot{\varphi}^2 \\ &\quad -R\, e\, m_2\, \cos(\theta)\, \dot{\varphi}\, \dot{\theta} + \left(\frac{m_2\, e^2}{2} + \frac{J_2}{2}\right) \dot{\theta}^2 \\ &\quad -e\, g\, m_2 + e\, g\, m_2\, \cos(\theta). \end{aligned} \tag{13}$$

This may be expressed compactly as

$$L = \frac{\hat{J}_1}{2}\dot{\varphi}^2 + a_R \cos(\theta)\, \dot{\varphi}\dot{\theta} + \frac{\hat{J}_2}{2}\dot{\theta}^2 + a_g\, (\cos(\theta) - 1), \tag{14}$$

where $\hat{J}_1 = J_1 + R^2\, (m_1 + m_2)$ is the effective moment of inertia of the wheel and inner frame about the contact point with the ground, $\hat{J}_2 = J_2 + e^2\, m_2$ is the moment of inertia of the inner frame about the centre of the wheels (from the parallel axis theorem), and $a_R = -R\, e\, m_2$ and $a_g = e\, g\, m_2$ are constants of convenience.

Euler-Lagrange equations

The dynamics are found from

$$\frac{d}{dt}\left(\frac{\partial L}{\partial \dot{\theta}}\right) - \frac{\partial L}{\partial \theta} + b_{12}(\dot{\theta} - \dot{\varphi}) = -\tau, \tag{15}$$

$$\frac{d}{dt}\left(\frac{\partial L}{\partial \dot{\varphi}}\right) - \frac{\partial L}{\partial \varphi} + b_{12}(\dot{\varphi} - \dot{\theta}) + b_1\dot{\varphi} = \tau, \tag{16}$$

where b_{12} is a viscous damping coefficient related to the relative velocities of the inner ring (θ) and the outer wheel (φ), b_1 is the viscous damping constant associated with the wheel rolling (and is surface dependent) and τ is a differential torque applied to both the inner ring and the outer wheel by the drive-wheel/motor assembly.

Evaluating the terms for θ

$$\frac{d}{dt}\left(\frac{\partial L}{\partial \dot{\theta}}\right) = \hat{J}_2\, \ddot{\theta} + a_R\, \ddot{\varphi}\, \cos(\theta) - a_R\, \dot{\varphi}\, \dot{\theta}\, \sin(\theta)$$

$$-\frac{\partial L}{\partial \theta} = \sin(\theta)\, \left(a_g + a_R\, \dot{\varphi}\, \dot{\theta}\right).$$

Evaluating the terms for φ

$$\frac{d}{dt}\left(\frac{\partial L}{\partial \dot{\varphi}}\right) = -a_R\, \sin(\theta)\, \dot{\theta}^2 + \hat{J}_1\, \ddot{\varphi} + a_R\, \ddot{\theta}\, \cos(\theta)$$

$$-\frac{\partial L}{\partial \varphi} = 0.$$

Differential Equations Therefore the governing differential equations of the diwheel are given by

$$-\tau = \hat{J}_2\, \ddot{\theta} + b_1\left(\dot{\theta} - \dot{\varphi}\right) + a_g\, \sin(\theta) + a_R\, \ddot{\varphi}\, \cos(\theta) \tag{17}$$

and

$$\tau = \hat{J}_1\, \ddot{\varphi} + b_{12}\, \left(\dot{\varphi} - \dot{\theta}\right) + b_1\dot{\varphi} - a_R\, \dot{\theta}^2\, \sin(\theta) + a_R\, \ddot{\theta}\, \cos(\theta). \tag{18}$$

It should be noted that the above differential equations are similar to the equations of motion derived for the monowheel by [Martynenko and Formal'skii, 2005; Martynenko, 2007] with the exception of the rolling resistance term b_1. It is also similar to that for the self-balancing two-wheel mobile robots [Grasser *et al.*, 2002; Ruan and Cai, 2009] and the ballbot [Lauwers *et al.*, 2006], where the only difference is that the gravitational term acts to stabilise the diwheel compared to the "inverted pendulum" robots which are unstable.

Solution to the Differential Equations of the Mechanical System

The system of differential equations may be solved in terms of $\ddot{\theta}$ and $\ddot{\varphi}$ to give

$$\begin{aligned} \ddot{\theta} &= -\frac{1}{D_1}\Bigg(\left(\hat{J}_1 + a_R \cos(\theta)\right)\left(\tau - b_{12}\dot{\varphi} - b_1\dot{\varphi} + b_{12}\dot{\theta}\right) \\ &\quad + a_R^2 \sin(\theta)\cos(\theta)\, \dot{\theta}^2 + \hat{J}_1 a_g \sin(\theta)\Bigg), \end{aligned} \tag{19}$$

where

$$D_1 = \hat{J}_1\, \hat{J}_2 - {a_R}^2 \cos^2(\theta), \tag{20}$$

and

$$\begin{aligned} \ddot{\varphi} &= \frac{1}{D_1}\Bigg(\left(\hat{J}_2 + a_R \cos(\theta)\right)\left(\tau - b_{12}\dot{\varphi} - b_1\dot{\varphi} + b_{12}\dot{\theta}\right) \\ &\quad + \hat{J}_2 a_R \sin(\theta)\, \dot{\theta}^2 + a_R a_g \sin(\theta)\cos(\theta)\Bigg). \end{aligned} \tag{21}$$

2.2 Fully Coupled Electro-Mechanical System

Electrical Dynamics

Permanent magnet DC electric motors have been used to power the diwheel. It has been assumed that the electrical inductance of the motors, L_m, is sufficiently small it may be neglected, and therefore the current in

the motor coil is an algebraic function of the supplied voltage V_m and motor speed $\dot{\theta}_m = Nn_s(\dot{\varphi} - \dot{\theta})$, and is given by

$$R_m i + K_m \dot{\theta}_m = V_m, \tag{22}$$

where R_m is the resistance of the armature, K_m is the *combined* motor torque constant (which is equal to the back EMF constant for SI units) for both motors, $N = \frac{R}{r}$ is the ratio of the wheel radius to drive-wheel radius and n_s is the drive ratio from the motor sprocket to drive-wheel sprocket (when using a chain drive).

The differential torque acting on the wheel and the inner frame generated by the motor in terms of the armature current is given by

$$\tau = Nn_s K_m i. \tag{23}$$

Combining Equations (22) and (23) gives the differential torque in terms of applied voltage

$$\tau = Nn_s K_m \left(V_m - Nn_s K_m (\dot{\varphi} - \dot{\theta}) \right) / R_m \tag{24}$$

Inserting Equation (24) into Equations (17) and (18) yields the differential equations of the fully coupled electro-mechanical system.

Solution to the Differential Equations of the Coupled Electro-Mechanical System

Equations (19) and (21) may be rewritten in terms of an input voltage to the motors by substituting Equation (24) to give

$$\begin{aligned} \ddot{\theta} &= -\frac{1}{D_1}\Bigg(\left(\hat{J}_1 + a_R \cos(\theta) \right) \\ &\times \left(\frac{Nn_s K_m}{R_m} V_m - (b_{12} + b_1 + b_m)\dot{\varphi} + (b_{12} + b_m)\dot{\theta} \right) \\ &+ a_R^2 \sin(\theta)\cos(\theta)\dot{\theta}^2 + \hat{J}_1 a_g \sin(\theta) \Bigg), \end{aligned} \tag{25}$$

where $b_m = \frac{(Nn_s K_m)^2}{R_m}$ is the effective damping from the back EMF, and

$$\begin{aligned} \ddot{\varphi} &= \frac{1}{D_1}\Bigg(\left(\hat{J}_2 + a_R \cos(\theta) \right) \\ &\times \left(\frac{Nn_s K_m}{R_m} V_m - (b_{12} + b_1 + b_m)\dot{\varphi} + (b_{12} + b_m)\dot{\theta} \right) \\ &+ \hat{J}_2 a_R \sin(\theta)\dot{\theta}^2 + a_R a_g \sin(\theta)\cos(\theta) \Bigg). \end{aligned} \tag{26}$$

2.3 Linearised Dynamics

The dynamics of the plant have been linearised about two operating conditions; the downward (stable) position and the upright (unstable) position.

Linearising about downward position

Using a Jacobian linearisation, the non-linear dynamics given by Equations (19) and (21) about the downward position $\theta = \dot{\theta} = \varphi = \dot{\varphi} = 0$ may be approximated by the linear state equations

$$\dot{\mathbf{x}} = \mathbf{A}\mathbf{x} + \mathbf{B}u, \tag{27}$$

where $\mathbf{x} = \begin{bmatrix} \theta & \varphi & \dot{\theta} & \dot{\varphi} \end{bmatrix}^T$ is the state vector, $u = \tau$ is the plant input and the state and input matrices are given by

$$\mathbf{A} = \frac{1}{{a_R}^2 - \hat{J}_1\hat{J}_2} \times \begin{bmatrix} 0 & 0 & 1 & 0 \\ 0 & 0 & 0 & 1 \\ \hat{J}_1 a_g & 0 & -a_R b_1 + (\hat{J}_1 + a_R)b_{12} & -(\hat{J}_1 + a_R)b_{12} \\ -a_g\, a_R & 0 & \hat{J}_2 b_1 - (\hat{J}_2 + a_R)b_{12} & (\hat{J}_2 + a_R)b_{12} \end{bmatrix} \tag{28}$$

and

$$\mathbf{B} = \frac{1}{{a_R}^2 - \hat{J}_1\hat{J}_2} \begin{bmatrix} 0 \\ 0 \\ (\hat{J}_1 + a_R) \\ -(\hat{J}_2 + a_R) \end{bmatrix}. \tag{29}$$

The poles of this plant are at $s = 0, -0.182, -0.23 \pm 2.60i$, with the complex poles having a damping ratio of $\zeta = 0.089$. The transfer function from τ to θ exhibits one zero on the origin which is expected as at the steady state $\theta(s \to 0) \to 0$. It is interesting to note that the transfer function from τ to φ exhibits two lightly-damped complex zeros at $s = -0.22 \pm 3.45i$. The presence of lightly damped complex zeros is similar to that found in other systems exhibiting slosh such as the ball and hoop system [Wellstead, accessed Aug 2009]. The implication is that if the motor is driven with a sinusoidal input at the frequency of the zeros, then the wheel will almost stand still and only the inner cage moves (when the damping is low).

Note that for the case of a voltage input, $u = V_m$, then the damping term arising from the differential velocity of the frame and wheel increases from $b_{12} \to b_{12} + b_m$ (resulting in open loop poles at $s = 0, -0.407, -0.47 \pm 2.52i$) and the state input matrix $\mathbf{B}$ needs to be multiplied by $\frac{Nn_s K_m}{R_m}$.

Linearising about upright (inverted) position

Linearising the non-linear dynamics given by Equations (19) and (21) about the upright position $\theta = \pi, \dot{\theta} = \varphi =$

$\dot{\varphi} = 0$ gives the linear state equations

$$\mathbf{A} = \frac{1}{{a_R}^2 - \hat{J}_1\hat{J}_2} \times \begin{bmatrix} 0 & 0 & 1 & 0 \\ 0 & 0 & 0 & 1 \\ -\hat{J}_1 a_g & 0 & a_R b_1 + (\hat{J}_1 - a_R)b_{12} & -(\hat{J}_1 - a_R)b_{12} \\ -a_g\, a_R & 0 & \hat{J}_2 b_1 - (\hat{J}_2 - a_R)b_{12} & (\hat{J}_2 - a_R)b_{12} \end{bmatrix} \tag{30}$$

and

$$\mathbf{B} = \frac{1}{{a_R}^2 - \hat{J}_1\hat{J}_2} \begin{bmatrix} 0 \\ 0 \\ (\hat{J}_1 - a_R) \\ -(\hat{J}_2 - a_R) \end{bmatrix}. \tag{31}$$

The poles of this plant are at $s = 0, -0.179, 2.29, -3.04$. Note that for the case of a voltage input, $u = V_m$, then the damping term arising from the differential velocity of the frame and wheel increases from $b_{12} \rightarrow b_{12} + b_m$ (resulting in open loop poles at $s = 0, -0.363, 2.00, -3.70$) and the state input matrix $\mathbf{B}$ needs to be multiplied by $\frac{N n_s K_m}{R_m}$ as per the downward linearisation case.

3 Control strategies

In this section a number of different control strategies are presented for the two-dimensional diwheel model. It should be noted that no literature to date has been published on control laws for either monowheels or diwheels. This is not surprising given that previous diwheels and most monowheels were human or IC engine driven which are not amenable to automatic control, the latter having dynamics with similar time constants to the plant.

The parameters used for the model, and thus the controller designs, are detailed in Table 1. Most parameters were estimated from the solid model of the diwheel (and rider) with the exception of the damping terms which were measured.

3.1 Slosh control

The purpose of the slosh controller is to minimise the amount of rocking (sloshing) that the driver experiences when rapidly accelerating or decelerating. This has parallels with slosh control in liquid-fueled rockets, ships and tankers [Aboel-Hassan *et al.*, 2009; Readman and Wellstead, accessed Aug 2009; Wellstead, accessed Aug 2009]. Any number of suitable linear and non-linear control strategies can be used to suppress the rocking (sloshing) motion of the diwheel. [Readman and Wellstead, accessed Aug 2009] fed back the slosh angle of a ball in a hoop (equivalent to θ in the diwheel) to restrict the slosh, which was equivalent to increasing the torque arising from the offset in the CoG of the inner frame. It was found that this technique is effective as it drives two complex closed loop poles towards the plant zeros. An alternative and obvious solution is to increase damping to reduce slosh using velocity feedback. Another common technique is input (also known as command) shaping, which involves modifying the reference command by convolving it with a set of self-destructive impulses that act against the complex poles in the plant. This approach is effectively pole-zero cancellation and is not robust.

Table 1: Parameters used to define the model. Note that the terms for the wheels and motors account for both acting together.

Part	Parameter	Value
Wheels	m_1	50.3 kg
	J_1	26.1 kg.m^2
Frame	m_2	218 kg
	J_2	48.4 kg.m^2
Lengths	R	720 mm
	$R_i \approx R$	720 mm
	r	140 mm
	e	160 mm
Damping	b_{12}	30 Nm.s/rad
	b_1	12 Nm.s/rad
Motor	V_{sat}	48 V
	R_m	0.628 Ohms
	L_m	0.3 mHenry
	K_m	65 mNm/A
Transmission	$N = \frac{R}{r}$	5.14
	n_s	7

The approach used here was simply to feed back the angular rate of the inner frame, $\dot{\theta}$. This decision was based on simplicity and availability of a state measurement from a solid state gyroscope. The final controller was

$$u = V_m = [\ 0 \quad 0 \quad 28 \quad 0\ ]\mathbf{x} = 28\dot{\theta}, \tag{32}$$

and was chosen to make the poles (of the linearised dynamics) entirely real. Note that the positive sign for this term arises from the fact that a positive motor torque leads to a negative acceleration of the inner frame (see Equation (19)).

3.2 Swing-up control

The swing-up controllers developed for other underactuated non-linear planar mechanical systems (such as the inverted pendulum) are applicable to the swing-up of the diwheel, since their dynamics are similar [Astrom and Furuta, 1996; Yoshida, 1999; Wang and Fang, 2004]. Almost all early works on swing-up controllers used a bang-bang switching approach to drive the po-

tential energy of the pendulum (in this case the inner frame) to the inverted state. More recently, fuzzy control has been used to swing-up (and balance) inverted pendulums [Martynenko and Formal'skii, 2005; Chang *et al.*, 2007]. In this paper two approaches will be investigated; a simple positive velocity feedback controller and a fuzzy controller.

Positive velocity feedback

One very simple strategy to swing the inner frame to the upright position is to simply move the complex poles from the left hand of the s-plane to the right hand side by feeding back a positive velocity of the motor (to make it go unstable), giving a controller of the form

$$u = V_m = [\ 0 \quad 0 \quad -10 \quad 10\ ]\mathbf{x} = 10\left(\dot{\varphi} - \dot{\theta}\right) = 10\frac{\dot{\theta}_m}{Nn_s}, \tag{33}$$

where the gains were chosen such that they were as large as possible without severely saturating the motors.

Fuzzy Controller

Fuzzy control has been applied to the problem of balancing the inverted pendulum, first by [Yamakawa, 1989]. Since then, various fuzzy logic controllers have been applied to various aspects of balancing problems. [Chang *et al.*, 2007] have described fuzzy controllers for both the swing-up and balancing control of a planetary train type pendulum. Their swing-up controller consists of a bang-bang control scheme, with little regard to the velocity of the pendant link - however this strategy is not immediately amenable to the diwheel system, since such a strategy tends to fight with gravity. Finally [Martynenko and Formal'skii, 2005] describe a fuzzy swing-up controller, which they have used to swing up a pendulum by emulating an energy based approach.

About the controller The fuzzy controller developed here uses two inputs from the physical system, the angular position of the inner ring with respect to earth (θ) and the rate of the inner ring ($\dot{\theta}$). The single output consists of a voltage between -48V and 48V. In contrast to previous fuzzy controllers applied to the inverted pendulum, this fuzzy controller does not aim to limit the horizontal travel of the diwheel, and the two chosen inputs appear appropriate for the problem of swinging the diwheel up.

Membership functions The membership functions of the two inputs are shown in Figure 4, and are similar to those presented in [Martynenko and Formal'skii, 2005]. The range of θ is $[-\pi, \pi]$ and the range of $\dot{\theta}$ is $[-2\pi, 2\pi]$. The output voltage membership function consists of five singleton sets corresponding to $[-48, -10, 0, 10, 48]$ Volts.

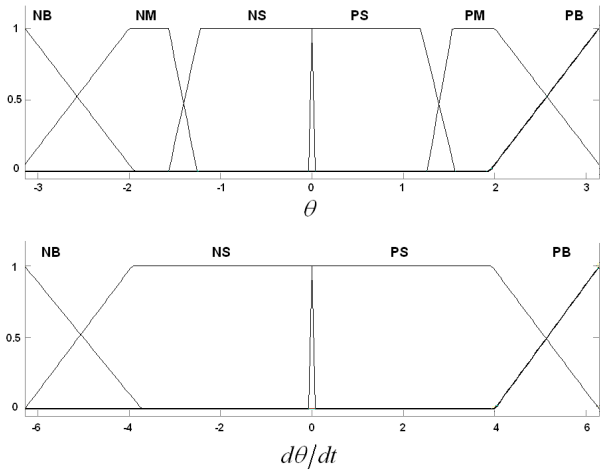

Figure 4: Membership functions

Rules The rules chosen for our initial fuzzy controller have been designed to force energy into the system in order to bring the inner ring to within $\pm 10°$of the inverted equilibrium point and are detailed in Table 2. The basic premise is to swing the inner ring hard until the back EMF of the motor develops sufficiently, and then to drive the motor so that it reinforces the fall of the inner ring due to gravity. For small angles ($|\theta| < \pi/2$) the action of the motor is determined according to the direction of the angular velocity, with regard to the fact that a positive motor voltage produces a negative reaction torque on the inner ring. For medium angles ($\pi/2 < |\theta| < 3\pi/4$) the motor is also driven hard when the angular velocity causes the inner ring to approach the balancing point. As the direction changes the motor direction is reversed. When the angle becomes large ($3\pi/4 < |\theta| < \pi$) and the angular rate is small, the motor action is made to cause the diwheel to 'drive underneath' the mass of the inner ring. For large angles and large angular rates the voltage is zero to allow the inner ring to slow down for capturing by the inversion controller.

3.3 Inversion control

A linear full-state feedback controller was used to keep the inner frame in the upright (open-loop unstable) position.

Linear Quadratic Regulator

A linear quadratic regulator (LQR) was used to stabilise the plant in its unstable position (Section 2.3). This approach has been used successfully in the inverted pendulum problem and its many variants [Lauwers *et al.*, 2006]. The cost function that was minimised is given by

$$J = \int_0^\infty \left(q_1\theta^2 + q_2\left(\dot{\theta} - \dot{\varphi}\right)^2 + R_1 V_m^2\right) dt \tag{34}$$

Table 2: Fuzzy rules

Rule 1	If (θ = PS) & ($\dot{\theta}$ = PS) then (V_m = NB)
Rule 2	If (θ = NS) & ($\dot{\theta}$ = NS) then (V_m = PB)
Rule 3	If (θ = PS) & ($\dot{\theta}$ = NB) then (V_m = PB)
Rule 4	If (θ = NS) & ($\dot{\theta}$ = PB) then (V_m = NB)
Rule 5	If (θ = PM) & ($\dot{\theta}$ = PB) then (V_m = NB)
Rule 6	If (θ = NM) & ($\dot{\theta}$ = NB) then (V_m = PB)
Rule 7	If (θ = PM) & ($\dot{\theta}$ = PS) then (V_m = NB)
Rule 8	If (θ = NM) & ($\dot{\theta}$ = NS) then (V_m = PB)
Rule 9	If (θ = PM) & ($\dot{\theta}$ = NB) then (V_m = NB)
Rule 10	If (θ = NM) & ($\dot{\theta}$ = PB) then (V_m = PB)
Rule 11	If (θ = PB) then (V_m = PS)
Rule 12	If (θ = NB) then (V_m = NS)
Rule 13	If (θ = PB) & ($\dot{\theta}$ = PB) then (V_m = Z)
Rule 14	If (θ = NB) & ($\dot{\theta}$ = NB) then (V_m = Z)

where q_1 and q_2 are the state penalties on the inner frame angle θ and the difference in the angular velocities between the frame and wheel $\dot{\theta} - \dot{\varphi}$ respectively. The purpose of the latter term is to restrict the speed of the drive motor which is rated to 2100RPM. The term R_1 is the penalty on the drive voltage. Using Bryon's rule, the state penalty matrix for the state vector given in Section 2.3 was set to

$$\mathbf{Q} = \begin{bmatrix} q_1 & 0 & 0 & 0 \\ 0 & 0 & 0 & 0 \\ 0 & 0 & q_2 & -q_2 \\ 0 & 0 & -q_2 & q_2 \end{bmatrix} = \begin{bmatrix} 36 & 0 & 0 & 0 \\ 0 & 0 & 0 & 0 \\ 0 & 0 & \frac{1}{36} & \frac{-1}{36} \\ 0 & 0 & \frac{-1}{36} & \frac{1}{36} \end{bmatrix} \tag{35}$$

and the effort penalty was

$$R_1 = \left(\frac{1}{\frac{1}{2}48} \right)^2 \tag{36}$$

Solving the continuous algebraic Riccati equation returns the optimal control gains

$$\mathbf{k} = [\ -209 \quad -4 \quad -57 \quad -32\ ]. \tag{37}$$

Pole placement (expensive control)
In parallel with the LQR controller described above, a state feedback regulator was developed by using the common method of pole placement. The placement involved reflecting all unstable poles about the imaginary axis so that they were stable. Note that this is equivalent to expensive LQR control, where the penalty on the control effort is infinite. The poles of the system were moved from those given in Section 2.3, viz. $s = 0, -0.363, 2.00, -3.70,$ to $s = 0, -0.363, -2.00, -3.70,$ resulting in a control vectors

$$\mathbf{k} = [\ -96 \quad 0 \quad -31 \quad -17\ ]. \tag{38}$$

4 Numerical Simulations

Numerical simulations were conducted on the differential equations derived in Section 2 within SIMULINK. To validate the differential equations and the implementation within SIMULINK, a parallel model was constructed using SIMMECHANICS. A virtual reality (VRML) model (shown in Figure 5) was built to aid in the visualisation of the plant.

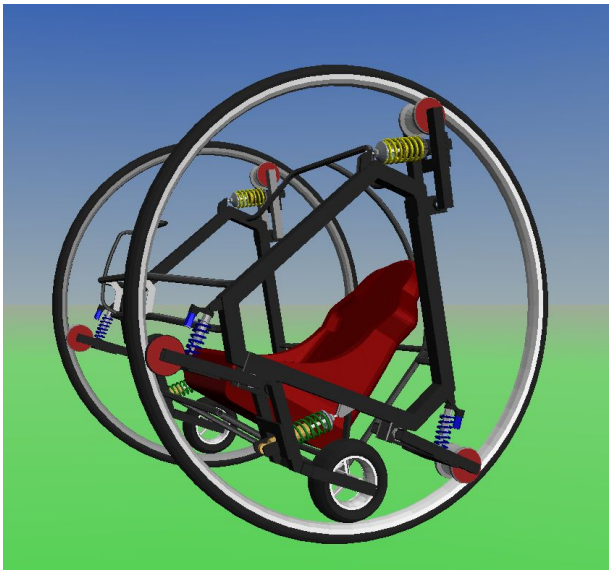

Figure 5: Rendered image of the VRML model

The various control strategies detailed in Section 3 were also integrated in to the SIMULINK model and the simulation results are presented following.

4.1 Open loop response

Figure 6 shows open loop response of the inner frame angle θ (and control voltage $V_m = 0$) when the inner frame was rotated to just less 180° and released. The slosh (rocking) is clearly evident.

4.2 Closed loop slosh control

Figure 7 shows the inner frame angle θ and control voltage V_m when the inner frame was rotated to just less 180°and released. Note that saturation of the motors just occurs and the slosh is dramatically curbed.

4.3 Swing-up control

The two swing-up controllers were investigated for the diwheel, when it was initially at rest and positioned at its stable equilibrium.

Positive velocity feedback
Figure 8 shows the response of the simple (positive velocity feedback) swing-up controller. Since it is based

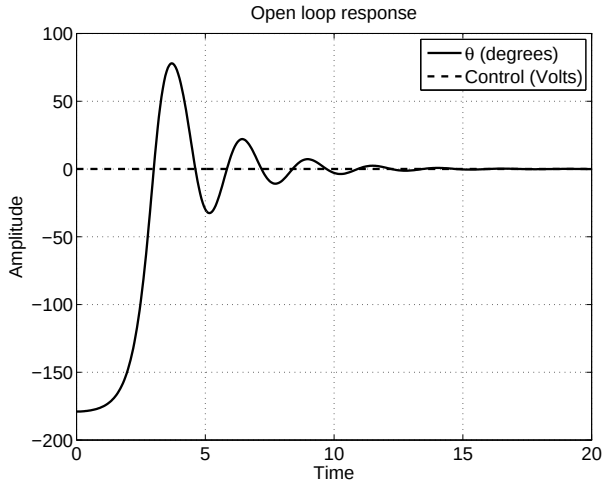

Figure 6: Open loop response when rotated to almost 180° and released

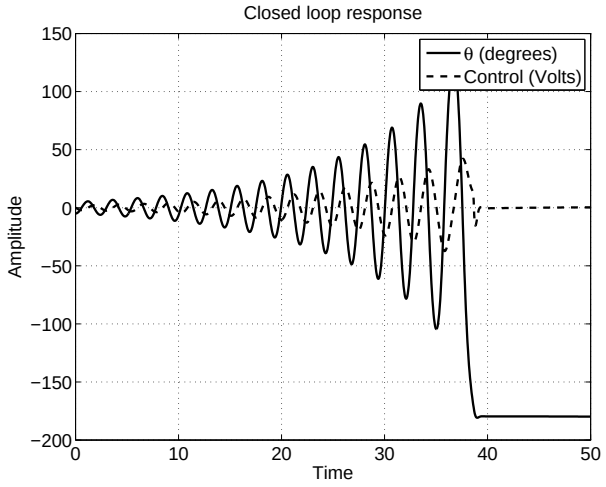

Figure 8: Closed loop response of positive velocity feedback swing-up controller

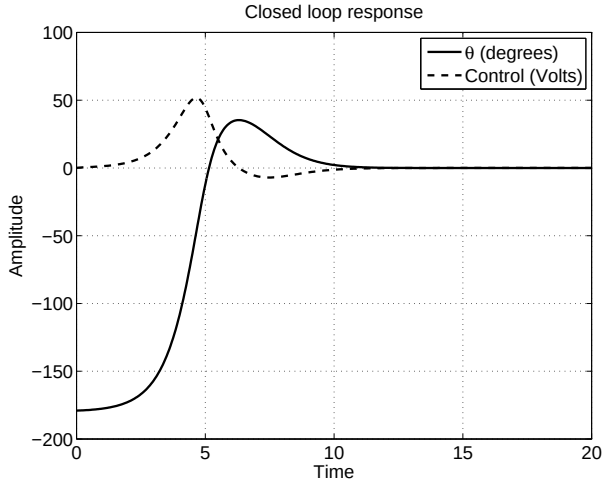

Figure 7: Closed loop response of slosh controller when rotated to almost 180° and released

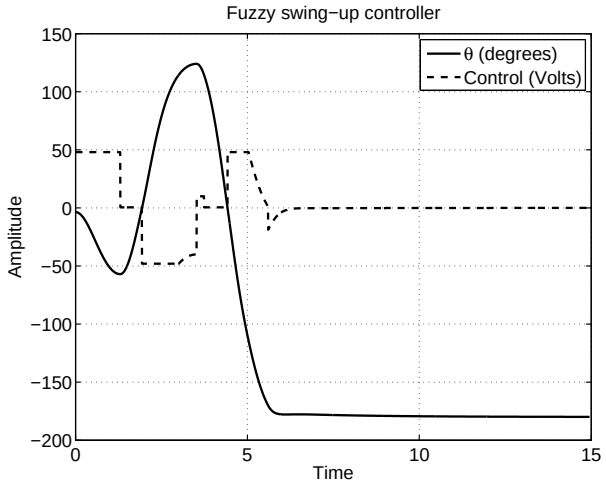

Figure 9: Closed loop response of fuzzy swing-up controller

on exponential growth (arising from the unstable pole), it takes a considerable time (38 seconds) to be captured by the inversion controller, even when starting from an initial state of $\theta_0 = 5°$.

Fuzzy controller

Figure 9 shows the response of the fuzzy swing-up controller. It can be seen from the magnitude of the control signal in Figure 8, that the simple method is no where near as effective as a bang-bang like fuzzy controller in Figure 9 for driving energy into the system.

4.4 Inversion control

Figure 10 shows the closed loop response of the frame angle θ and the control signal V_m to an initial pose of $\theta_0 = 170°$ when using the LQR given by Equation (37). The expensive control gains given by Equation (38) were analysed, and although they were able to stabilise the plant, the non-aggressive control law was unable to capture the inner frame upon swing-up for all but the most benign cases.

5 Conclusion and Future Work

In this paper the dynamics of the diwheel were derived, where it was seen that it exhibits behaviour seen in other nonlinear under-actuated unstable mechanical plants such as the inverted pendulum and self-balancing wheeled robots [Fantoni and Lozano, 2001]. Consequently, approaches applied to systems with similar dynamics are also applicable to the diwheel, which have been successfully demonstrated here.

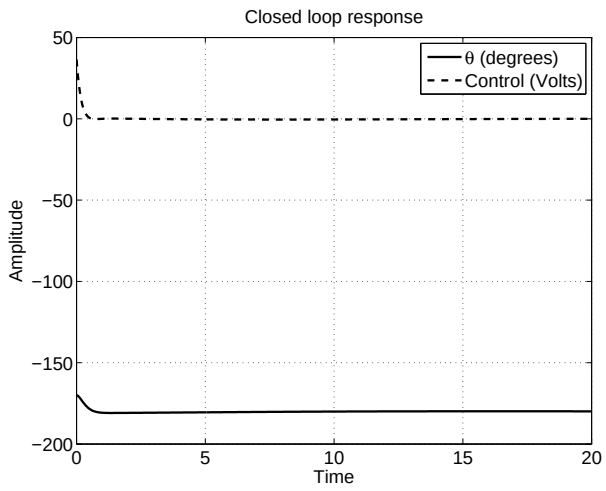

Figure 10: Closed loop response of inversion controller to an initial pose of $\theta_0 = 170°$

Future work will involve extension of the two-dimensional model to a fully coupled three-dimensional model, including yaw arising from differential motion of the wheels. In parallel to this work will also continue on the EDWARD diwheel, including the final assembly and commissioning, conducting a thorough system identification, testing the different safety systems, and then finally implementing and benchmarking the various control strategies.

Acknowledgments

The authors would like to acknowledge the support of the Bob Dyer and Phil Schmidt for their efforts in constructing the physical diwheel used as the basis of the model in this paper.

References

[Aboel-Hassan *et al.*, 2009] A. Aboel-Hassan, M. Arafa, and A. Nassef. Design and optimization of input shapers for liquid slosh suppression. *Journal of Sound & Vibration*, 320:1–15, 2009.

[Astrom and Furuta, 1996] K.J. Astrom and K. Furuta. Swinging up a pendulum by energy control. In *IFAC 13th World Congress*, 1996.

[Cardini, 2006] S.B. Cardini. A history of the monocycle - stability and control from inside the wheel. *IEEE Control Systems Magazine*, 26(5):22–26, 2006.

[Chang *et al.*, 2007] Y.-H. Chang, C.-W. Chang, C.-H. Yang, and C.W. Tao. Swing up and balance control of planetary train type pendulum with fuzzy logic and energy compensation. *International Journal of Fuzzy Systems*, 9(2):87–94, 2007.

[Dyer *et al.*, 2009] C. Dyer, K. Fulton, J. Harvey, E. Schumann, and C. Zhu. Electric Di-Wheel with Automatic Rotation Damping. Technical report, The University of Adelaide, 2009.

[Fantoni and Lozano, 2001] I. Fantoni and R. Lozano. *Non-linear Control for Underactuated Mechanical Systems*. Springer, 2001.

[Grasser *et al.*, 2002] F. Grasser, A. D'Arrigo, S. Colombi, and A.C. Rufer. Joe: A mobile, inverted pendulum. *IEEE Transactions on Industrial Electronics*, 49(1):107–114, 2002.

[Lauwers *et al.*, 2006] T.B. Lauwers, G.A. Kantor, and R.L. Hollis. A dynamically stable single-wheeled mobile robot with inverse mouse-ball drive. In *IEEE Int. Conference on Robotics and Automation*, pages 2884–2889, Orlando, FL., 2006.

[Martynenko and Formal'skii, 2005] Y.G. Martynenko and A.M. Formal'skii. Theory of the control of a monocycle. *Applied Mathematics and Mechanics*, 69(4):516–528, 2005.

[Martynenko, 2007] Y.G. Martynenko. Motion control of mobile wheeled robots. *Journal of Mathematical Sciences*, 147(2):6569–6606, 2007.

[Readman and Wellstead, accessed Aug 2009] M. Readman and P. Wellstead. Ball and hoop 2: Control and analysis. Technical report, Controlsystems-principles.co.uk., accessed Aug. 2009.

[Ruan and Cai, 2009] X. Ruan and J. Cai. Fuzzy backstepping controllers for two-wheeled self-balancing robot. In *International Asia Conference on Informatics in Control, Automation and Robotics*, 2009.

[Self, accessed Aug 2009] D. Self. Dicycles and diwheels. [Online - www.dself.dsl.pipex.com/MUSEUM/TRANSPORT], accessed Aug. 2009.

[Wang and Fang, 2004] Chen Y. Wang, Z. and N. Fang. Minimum-time swing-up of a rotary inverted pendulum by iterative impulsive control. In *American Control Conference*, pages 1335–1340. IEEE, 2004.

[Wellstead, accessed Aug 2009] P. Wellstead. Ball and hoop 1: Basics. Technical report, Control-systems-principles.co.uk., accessed Aug. 2009.

[Yamakawa, 1989] T. Yamakawa. Stabilization of an inverted pendulum by a high-speed fuzzy logic controller hardware system. *Fuzzy Sets and Systems*, 32(2):161–180, 1989.

[Yoshida, 1999] K. Yoshida. Swing-up control of an inverted pendulum by energy-based methods. In *American Control Conference*, pages 4045–4047, 1999.